Acta Materialia 188 (2020) 101–107

Contents lists available at ScienceDirect

Acta Materialia

journal homepage: www.elsevier.com/locate/actamat

Full length article

Modeling zirconia sintering trajectory for obtaining translucent submicronic ceramics for dental implant applications

Charles Manière[a,*], Geuntak Lee[a,b], Joanna McKittrick[b,1], Shirley Chan[a], Eugene A. Olevsky[a,c]

[a] Powder Technology Laboratory, San Diego State University, San Diego, United States
[b] Mechanical and Aerospace Engineering, University of California, La Jolla, San Diego, United States
[c] NanoEngineering, University of California, La Jolla, San Diego, United States

ARTICLE INFO

Article History:
Received 29 October 2019
Revised 17 January 2020
Accepted 30 January 2020
Available online 5 February 2020

Keywords:
Modeling
Sintering trajectoryt
Translucent
Dental implant
Two step sintering
Zirconia

ABSTRACT

Attaining high densification without grain growth is one of the main objectives of the sintering optimization in ceramic materials. For dental implant applications, achieving this objective has a decisive impact on the mechanical resistance, the duration and the translucency of the implant. To improve these sintering outcomes a long experimental explorative study is generally required. In this work, we developed a combined experimental/modeling approach allowing a rapid identification of the optimal sintering conditions. The determination of the model densification and grain growth kinetic constitutive parameters has been done experimentally. We found that the sintering/grain growth kinetics have a detrimental acceleration above a critical temperature level. The pressure-less sintering model able to predict the sintering stress, powder densification and grain growth has been used for the determination of the optimal sintering trajectory. We utilized the two step sintering method to approach the critical temperature without an undesirable grain growth. We obtained translucent sintered specimens with a very limited grain growth.

1. Introduction

Attaining a final high relative density and a minimum of grain growth are required sintering outcomes for obtaining translucent zirconia dental implants with high mechanical strength [1–5]. Pressures-less sintering modeling is an efficient way to optimize the grain growth/densification sintering trajectory for different thermal cycles. It requires a careful identification of the densification/grain growth during the final stage of sintering. Grain growth is known to slow down the sintering kinetics by increasing the diffusion distances [6–8]. The traditional sintering models consider a particle size and porosity dependence of the effective sintering stress [9]. Also, grain growth induces longer diffusion distances within the grain's bulk and at the grain boundaries [6]. This phenomenon is particularly known for diffusional creep, where larger grains are associated with slower creep rates (at the same temperature) due to longer grain boundaries or lattice diffusion distances. The grain growth kinetics is known to be affected by porosity (porosity pinning), which results in the different grain growth mechanisms for high and low porosity stages of sintering [6,7]. In the generalized form of the continuum theory of sintering, it is usually assumed that the grain growth modifies the sintering stress and the material's equivalent deformation behavior (viscosity for linear viscous constitutive behavior, and the creep properties for nonlinear viscous constitutive behavior) [10]. The prediction of the densification/grain growth kinetics and their interaction during the sintering process is the key for understanding the sintering final stage phenomena [8,11]. For spark plasma sintering [12], the information on the densification/grain growth interaction can be used to optimize the densification curve at the end of the cycle [13].

In this work, we investigate the possibility to predict by an analytic sintering/grain growth model the sintering trajectory of a zirconia powder dental implant. In this regard, the implant should simulate the translucent aspect of natural teeth and have high mechanical properties to resist the chewing stress and to extend the implant duration [5]. Minimal porosity and grain sizes are required to optimize these characteristics. First, we will explore the implant material's experimental sintering response (in terms of porosity and grain size) under different sintering temperatures and holding cycles. Based on this, the sintering/grain growth model will be calibrated to follow the experimental data points and the explored sintering trajectory. When the model renders a satisfactory response, it will be employed to virtually adjust different sintering cycles using long holding times (a long exploration time would be needed if the material were tested experimentally). We will, in particular, explore the two step sintering method to

* Corresponding author: C. Manière, Powder Technology Laboratory, College of Engineering, San Diego State University, 5500 Campanile Drive, San Diego, CA 92182-1323.
E-mail addresses: charles.maniere@ensicaen.fr, charles.maniere@hotmail.fr (C. Manière).
[1] Posthumous contribution.

https://doi.org/10.1016/j.actamat.2020.01.061
1359-6454/

Nomenclature

θ	Porosity
$\dot{\theta}$	Porosity elimination rate (s^{-1})
$\underline{\sigma}$	Stress tensor (N.m^{-2})
$\underline{\dot{\varepsilon}}$	Strain rate tensor (s^{-1})
$\dot{e}$	Trace of the strain rate tensor (s^{-1})
$\dot{\varepsilon}_r$	Radial component of isotropic strain rate tensor (s^{-1})
φ	Shear modulus
ψ	Bulk modulus
P_l	Sintering stress (Pa)
i	Identity tensor
α	Surface energy (J.m^{-2})
r	Particle mean radius (m)
η	Material viscosity (Pa.s)
η_0	Viscosity pre-exponential factor (Pa.s)
Q	Viscosity activation energy (J.mol^{-1})
R	Gas constant 8.314 (J.mol^{-1}.K^{-1})
T	Temperature (K)
$\dot{G}$	Grain growth rate (m.s^{-1})
G	Grain size diameter (m)
G_0	Initial grain size diameter (m)
p	Grain growth rate exponent
K	Grain growth factor (m^{1+p}.s^{-1})
k_0	Grain growth pre-exponential factor (m^{1+p}.s^{-1})
Q_G	Grain growth activation energy (J.mol^{-1})
m	Viscosity grain size exponent
C	Constant
w	Sintering equation grain size exponent
D	Diffusion coefficient
k	Boltzmann constant (1.38064852E-23 J.K^{-1})

optimize the sintering trajectory [14]. Then the optimized cycle will be tested experimentally for verification.

2. Theory and calculations

The sintering model employed is based on the continuum theory of sintering [9]. This approach allows an easy identification of the sintering parameters using the analytic constitutive equations and provides the possibility to use these parameters in finite element simulations. The constitutive equation describing the linear viscous densification behavior of a compressible medium taking into account the sintering stress P_l is defined as:

$$\underline{\sigma} = 2\eta\left(\varphi\underline{\dot{\varepsilon}} + \left(\psi - \frac{1}{3}\varphi\right)\dot{e}\mathrm{i}\right) + P_l\mathrm{i} \tag{1}$$

with the invariant (volumic shrinkage rate):

$$\dot{e} = \dot{\varepsilon}_x + \dot{\varepsilon}_y + \dot{\varepsilon}_z \tag{2}$$

and the Skorohod's sintering stress expression [15] for the capillarity forces developed at the particles contacts:

$$P_l = \frac{3\alpha}{r}(1-\theta)^2 \tag{3}$$

Eq. (1) gives the sintering deformation behavior of a linear viscous medium. The porosity evolution rate is linked to the rate of volume change through the mass conservation equation:

$$\frac{\dot{\theta}}{1-\theta} = \dot{\varepsilon}_x + \dot{\varepsilon}_y + \dot{\varepsilon}_z \tag{4}$$

For pressure-less isotropic sintering, the stress and strain rate tensors can be reduced to:

$$\underline{\sigma} \equiv \begin{pmatrix} 0 & 0 & 0 \\ 0 & 0 & 0 \\ 0 & 0 & 0 \end{pmatrix}; \underline{\dot{\varepsilon}} \equiv \begin{pmatrix} \dot{\varepsilon}_r & 0 & 0 \\ 0 & \dot{\varepsilon}_r & 0 \\ 0 & 0 & \dot{\varepsilon}_r \end{pmatrix} \text{ isotropic } \dot{e} = 3\dot{\varepsilon}_r \tag{5}$$

Eq. (1) and (5) give the following radial tensor component expression:

$$0 = 2\eta\left(\varphi\dot{\varepsilon}_r + \left(\psi - \frac{1}{3}\varphi\right)3\dot{\varepsilon}_r\right) + P_l \tag{6}$$

We obtain the reduced expression:

$$-P_l = 2\eta 3\dot{\varepsilon}_r\psi \tag{7}$$

Using the mass conservation (4), we obtain [9]:

$$\psi = \frac{-P_l(1-\theta)}{2\eta\dot{\theta}} \tag{8}$$

and then, the analytic equation describing the rate of porosity elimination [9];

$$\dot{\theta} = \frac{-P_l(1-\theta)}{2\eta\psi} \tag{9}$$

Eq. (9), can be used to model the sintering densification. However, at the sintering final stage, the grain growth will influence the sintering stress (3) and the viscosity. The grain growth kinetics is usually modeled by the following equation [6,7,16]:

$$\dot{G} = \frac{K}{G^p} = \frac{k_0}{G^p}exp\left(\frac{-Q_G}{RT}\right) \tag{10}$$

Based on the linear diffusional creep mechanisms, the viscosity temperature and grain size dependence can be defined by the expression [8,11,13,17]:

$$2\eta = \left(\frac{G}{G_0}\right)^m \eta_0 T\exp\left(\frac{Q}{RT}\right) \tag{11}$$

If we assume the presence of no hard agglomerates, a dense and homogeneous initial packing of the grains and a homogeneous distribution of the porosity, then the effective particle size responsible for sintering should be close to the grain size. Substituting the expression of the sintering stress (3) and the viscosity (11) in Eq. (9), we obtain the expression of the rate of porosity evolution which takes into account the actual grain size (G).

$$\dot{\theta} = \frac{-6\alpha(1-\theta)^3}{G^{m+1}\frac{\eta_0}{G_0^m}T\exp\left(\frac{Q}{RT}\right)\psi} \tag{12}$$

This equation can be compared to the theoretical equations of solid-state sintering which have the general form [6,18–20]:

$$\dot{\theta} = \frac{-C\,f(\theta)\alpha D}{G^w kT} \tag{13}$$

In this equation, C is a constant, $f(\theta)$ a function of the porosity, and D the diffusion coefficient (D_v for volume diffusion and $\delta_{gb}D_{gb}$ for grain boundary diffusion) which has an Arrhenius form. From Coble [21] sintering models and in accordance with Herring's scaling law [22], the grain size exponent w in (13) has a value of 4 for grain boundary diffusion and 3 for volume diffusion [6]. Comparing Eq. (12) based on the continuum modeling approach and Eq. (13) based on the combined stage analytical sintering model [23], we can see that all the constants (G_0, m, k, η_0) of Eq. (12) are included in C constant, the exponential term is included in the diffusion coefficient, $f(\theta)$ gather all the porosity terms in Eq. (12) including the bulk modulus ψ and the sintering stress porosity function, and we have,

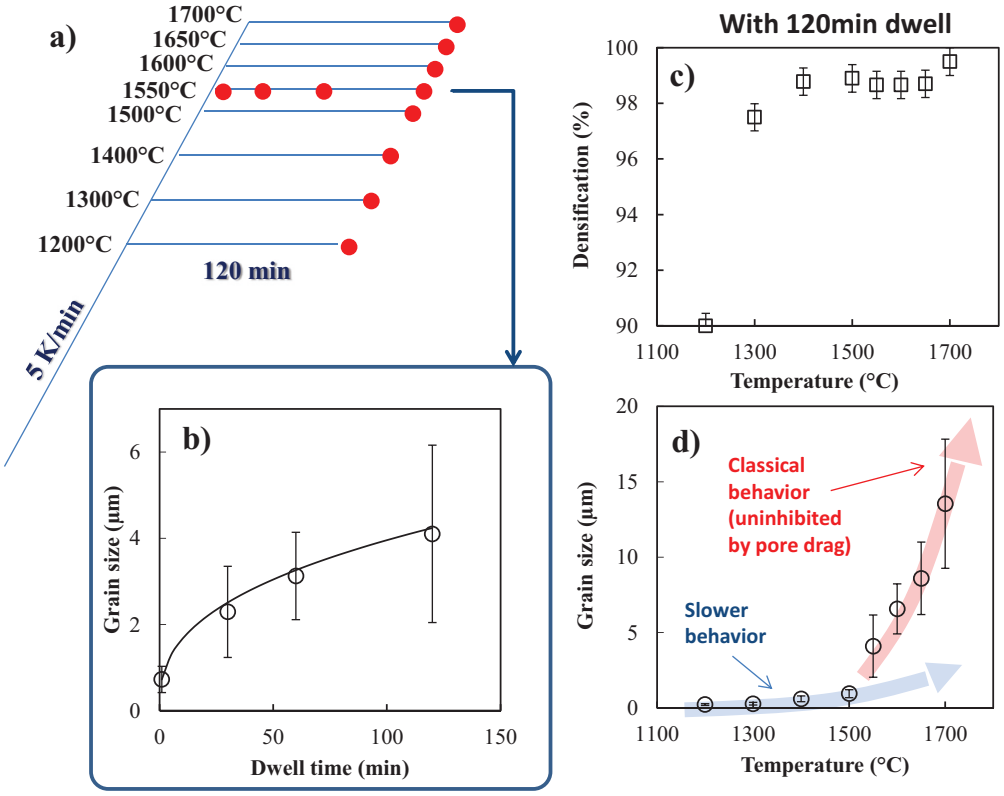

Fig. 1. Experimental exploration of Zpex Smile zirconia pressure-less sintering, (a) sintering cycles, (b) grain size evolution in 1550 °C tests, (c) densification of the specimens obtained with 120 min dwell, (d) average grain size of 120 min dwell specimens at different temperatures.

$w = m + 1$. The analytic form of the sintering kinetic Eqs. (13) or (12) is very useful to predict the sintering responses of numerous ceramics powders, for instance via the 'Wang and Raj' [20] or 'master sintering curve' [24,25] experimental methods. The use of these analytical equations is possible for a system having homogeneous distribution of porosity and grain sizes. In this paper, we show the possibility of optimizing the sintering trajectory by an experimental identification of the densification/grain growth behavior. For this purpose, the sintering parameters of Eqs. (10) and (12) will be experimentally identified based on different sintering conditions (temperatures, holding time) based on a successful reproduction of the sintering response (porosity, grain size). Then, this model will be used to virtually explore the optimal sintering trajectory in the temperature range where the model was identified.

In order to determine the viscosity parameters and the surface energy, Eq. (12) was written in the form (14) below, enabling the constitutive parameters' identification by a linear regression. Eq. (14) is obtained for the intermediate stage of sintering where the sintering kinetic is not influenced by the grain growth. In this region (between 50–87% of density), the ratio $\frac{G}{G_0}$ in the viscosity equation is 1 and Eq. (12) can be reduced to the following form which enables the viscosity term identification by linear regression.

$$Y = ln\left(\frac{-3(1-\theta)^3}{rT\dot{\theta}\psi}\right) = ln\left(\frac{\eta_0}{\alpha}\right) + \frac{Q}{RT} \tag{14}$$

3. Experiment and method

This study employs Tosoh Zpex Smile zirconia (3 Y_2O_3 mol%) powder specimens prepared by 200 MPa Cold Isostatic Pressing (CIP American isostatic pressing). The 'Zpex Smile' powder grade of Tosoh is specifically designed for improving the aggregation of particles resulting in higher light transmittance of the translucent sintered ceramic [26]. In order to identify the sintering densification behavior using Eq. (14), a dilatometry test was performed (Unitherm model 1161, Anter Corporation) at 5 K/min up to 1650 °C. For the determination of the grain growth kinetics, we conducted different sintering tests with a 5 K/min heating ramp and two hours of holding at different temperatures. To determine the grain growth rate exponent p, we conducted interrupted dwell experiments for a temperature level at the onset of grain growth in the sintering trajectory (1550 °C see later). The mean grain diameter was calculated through the scanning electron microscopy (SEM FEI Quanta 450, USA) of polished and thermally etched samples; the linear intercept method using Mendelson's stereological factor (1.56) was used [27]. After obtaining the average grain size and the relative density of all samples, the grain growth rate exponent p and K factor were determined for the interrupted sintering tests at 1550 °C. Then, the sintering data obtained using Eq. (14)-based regression of the dilatometry test was employed to simulate all the sintering experiments. The model of sintering during the final stage was particularly adjusted using the grain growth relationship to determine the grain growth activation energy Q_G. After a reasonable prediction of all the sintering tests at different temperatures, the densification and grain growth data were used to determine an optimized sintering cycle.

4. Results and discussions

4.1. Sintering tests

The sintering process design and obtained specimens' average grain sizes and relative density are reported in Fig. 1. The experimental process design consists of a sintering cycle with a heating ramp of 5 K/min and a 2 hours holding time under temperatures between 1200 and 1700 °C (see Fig. 1(a)). The experiments at 1550 °C were carried out at different holding times to reveal the isothermal grain growth

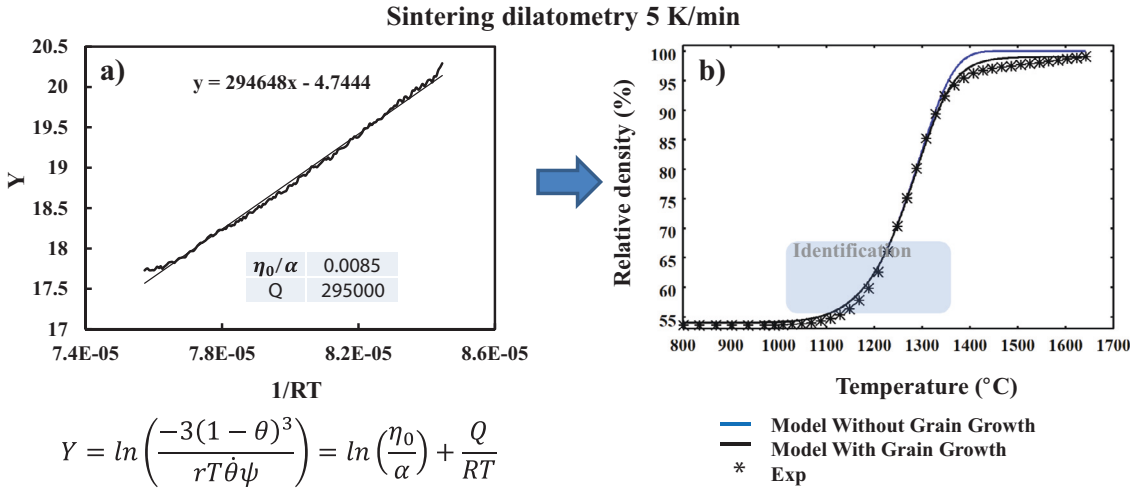

Fig. 2. Identification of the densification behavior based on 5 K/min sintering dilatometry (a) and experimental densification data modeled with and without grain growth (b).

behavior (see Fig. 1(b)). For the different tests conducted with 2 hours of holding time, the average relative densities and grain sizes are reported in Fig. 1((c) and (d)). It is interesting to note in Fig. 1(d) two different grain growth behaviors: a slow grain growth behavior for temperatures below 1550 °C and a behavior which has faster grain growth kinetics for higher temperatures. A possible explanation of this change of the grain growth behavior could be a slower grain growth kinetics due to the intergranular porosity pinning which slows down the grain boundary mobility [6,7]. The grain growth curves (Fig. 1(d)) and the densification data (Fig. 1(c)) show that this transition cannot by easily related to the specimen's overall densification, but it seems more influenced by the temperature which accelerates the grain boundaries' mobility. This slower grain growth zone is of high importance for our study which is essentially focused on the slow kinetics zone (blue arrow in Fig. 1(d) with low grain boundary mobility) to eliminate the porosity with a minimum of the grain growth. It is important to avoid the formation of an intragranular porosity which is known to be very difficult to eliminate [6,7].

4.2. Identification of the modeling parameters

4.2.1. Sintering dilatometry

An important step of this study is to determine the densification parameters of the employed powder during the 5 K/min heating ramp. Our entire study is focused on this typical heating ramp to avoid the potential heating rate contribution [28] like surface diffusion, coarsening [19], and extensive constitutive parameter identification tests. A sintering dilatometry is performed for this heating ramp. The densification data ($\dot{\theta}$, θ) are extracted to plot based on Eq. (14) the regression graph of Fig. 2(a) which gives the ratio η_0/α of 0.0085 Pa.m^2.s.J^{-1}.K^{-1} and the densification activation energy Q of 295 kJ.mol^{-1}. The sintering constitutive parameter identification zone is reported in Fig. 2(b) and represents an area where the grain growth is not active. This graph also reports the model of the dilatometry test with and without grain growth. The modeled sintering curve without grain growth is calculated by considering a constant grain size (Eq. (10) is reduced to $\dot{G} = 0$). This shows the influence of the grain growth at the end of the sintering cycle where the sintering rate is decreased.

4.2.2. Grain growth at 1550 °C

To estimate the grain growth rate exponent p, the interrupted dwell tests were carried out under 1550 °C (during the transition of the grain growth behavior). Using Eq. (10) in a logarithm form and the data in Fig. 1(b), it is possible to determine the grain growth rate exponent p and the pre-exponential factor K for 1550 °C by a regression

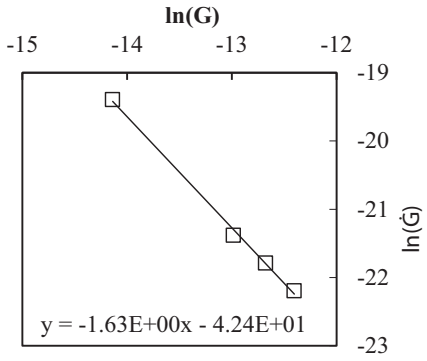

Fig. 3. Grain growth parameters identification at 1550 °C.

approach reported in Fig. 3. We obtained the value p of 1.63 (which corresponds to a boundary controlled grain growth mechanism in a pure or doped system ~2 [6]) and a K value of 3.74E-19 m^{1+p}.s^{-1}. We use these data to calibrate k_0 and Q_G corresponding to the generalized grain growth behavior (the data of Fig. 1) and the analytical model which utilizes Eqs. (4, 10, 12) and assumes the dominant grain boundary diffusion densification mechanism [6,20].

4.2.3. Grain growth below 1550 °C

Using the densification parameters of Fig. 2, the sintering/grain growth analytical model was employed to calibrate the grain growth behavior (k_0 and Q_G) with the grain size data below 1550 °C. The results are reported in Fig. 4. One can see that the 1200 °C experiment has almost no grain growth and an incomplete densification. The grain growth kinetics is slow until 1300 °C where it becomes active. In the temperature zone of Fig. 4 we obtained the grain growth parameters of k_0 = 1.5E-4 m^{1+p}.s^{-1} and Q_G = 600 kJ.mol^{-1} (close to the 546 kJ.mol^{-1} obtained by Chaim [29] above 1400 °C). These values are of high importance for the sintering optimization study because they represent the grain growth kinetics in the transition from high to low porosities.

4.2.4. Grain growth above 1550 °C

In order to predict the grain growth for higher temperatures, the grain growth model has been also calibrated for temperatures above 1550 °C. The results are reported in Fig. 5. Because the temperatures are within a high range, the main part of the densification is conducted during the 5 K/min heating ramp and the grain growth dominates the high temperature densification. In consequence, the densification occurs up to 97.5% of the relative density regardless of

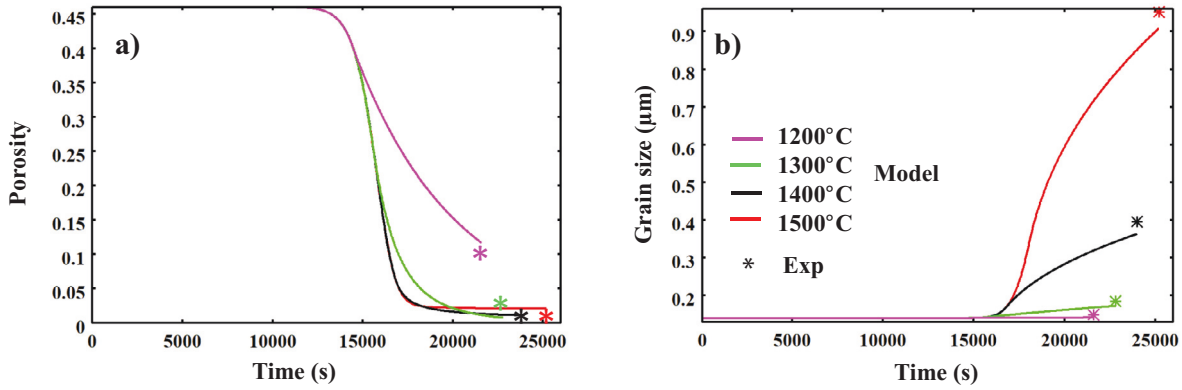

Fig. 4. Identification of the grain growth kinetics below 1550 °C, (a) modeled porosity evolution, (b) modeled grain size evolution.

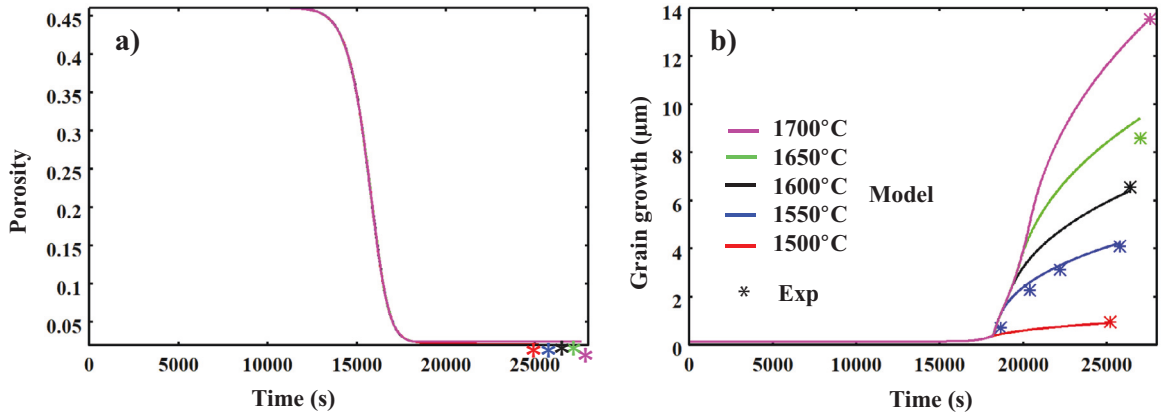

Fig. 5. Identification of the grain growth kinetics above 1500 °C, (a) modeled porosity evolution, (b) modeled grain size evolution.

the temperature cycle (see Fig. 1(c)). This phenomenon is observed experimentally (Fig. 1(c)) where the final relative density seems to stabilize close to 98.6% for temperatures above 1400 °C. We obtained the following grain growth values: k_0=0.058 $m^{1+p}.s^{-1}$ and Q_G = 600 kJ.mol^{-1}.

4.2.5. Thermal transition of the grain growth behavior

In the generalized grain growth model, we chose to model the transition from the low to high temperature behaviors via a sigmoidal function (15) which gives 0 for low temperatures and 1 for high temperatures.

$$f0 = \frac{1}{1 + exp(-0.1(T - Tcr))} \tag{15}$$

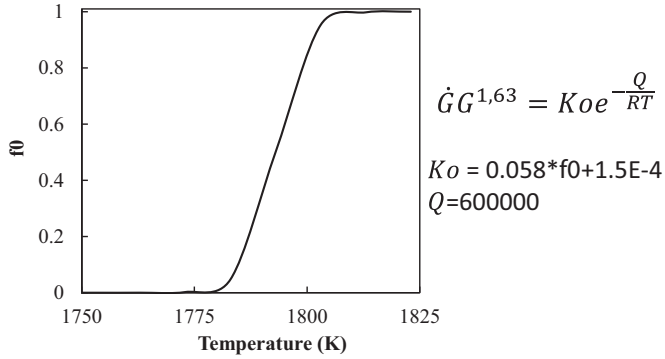

Fig. 6. Sigmoidal function used to model the grain growth behavior transition between 1500 and 1550 °C.

Based on the results in Fig. 1(d), the critical temperature *Tcr* was chosen to be 1520 °C. This function is reported in Fig. 6. This grain growth rate transition with temperature also appears in Chaim's results [29] and is here modeled by f0. At this stage, the sintering/grain growth model is fully identified, and the sintering optimization can be conducted using the determined constitutive parameters.

4.3. Modeling of optimized sintering trajectories

The modeling optimization study is conducted using the two step sintering method. This method consists of an initial heating to a maximum temperature followed by a temperature decrease down to a long holding temperature which is lower than the maximum temperature attained at the end of the initial heating ramp. This approach has shown an interesting potential for the improvement of the sintering trajectory without the help of an externally applied pressure [14]. In the present study, (see Fig. 7(a)) a 5 K/min heating ramp is applied to the highest temperature under which the grain growth is not highly active (1400 °C). After reaching this temperature, a 5 K/min decrease is applied to reach different lower temperatures held during 10 hours to ensure a slow but active densification. The two steps sintering approach is used to simplify the optimization study as the experiments (Fig. 1(a)) clearly indicate the critical temperature at which the grain growth accelerates.

The obtained porosity and grain size evolution curves are reported in Figs. 7(a) and 7(b), respectively. From the modeled sintering trajectory reported in Fig. 7(d), one can see that the optimal sintering cycle having a maximal densification for a limited grain growth corresponds to the cycle with a holding temperature of 1300 °C. One can clearly see that the regular one-step sintering cycle (in red) causes an excessive grain growth which prevents attaining high densification.

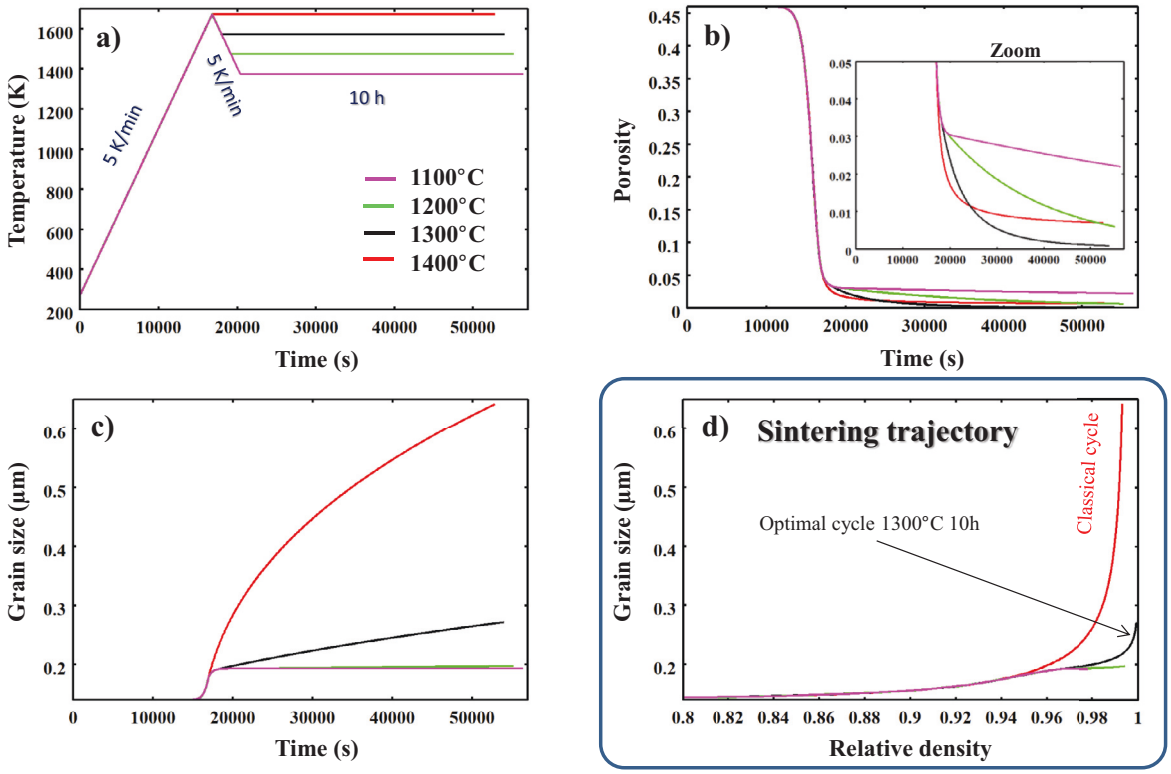

Fig. 7. Modeled sintering trajectories for the optimization of the sintering of the zirconia samples through the two step sintering approach, (a) Temperature cycles, (b) modeled porosity evolution, (c) modeled grain size evolution, (d) modeled sintering trajectories.

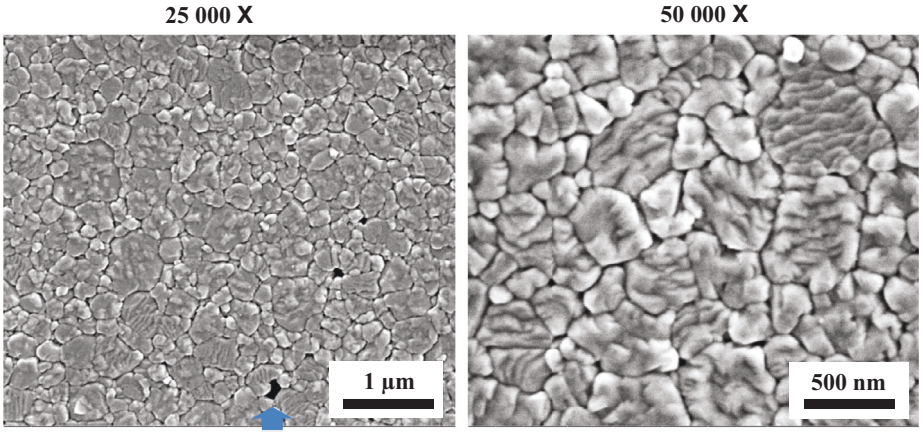

Fig. 8. Experimental microstructure obtained by SEM at two magnifications for the optimized sintering cycle predicted by modeling.

4.4. Experimental test using the optimized sintering cycle

The results obtained by modeling optimal sintering cycle at 1300 °C have been tested experimentally. The respective microstructure is reported in Fig. 8. The average grain size is 285 nm (±153 nm of standard deviation), which is close to the 272 nm obtained in the modeling approach. The presence of localized porosity (99.3% of densification) is observed (blue arrow) while the model predicted a quasi-full densification. However, this experimentally observed porosity seems to be very localized and can be caused by compaction defects or impurities which can generate a similar porosity not homogeneously distributed around the grains (and not predicted by the model).

5. Conclusions

A coupled sintering/grain growth model has been developed based on the continuum theory of sintering and applied to the optimization of sintering of zirconia powder used for dental implant applications. Constitutive equations have been derived for the modeling study and for the identification of the sintering and grain growth constitutive parameters. The sintering experiments performed under different temperatures reveal that the grain growth has two types of behaviors. The first behavior represents the slow grain growth for low temperatures, which can be possibly explained by the pore pinning of the grain boundaries, and the second behavior corresponds to the faster grain growth kinetics for temperatures higher than 1550 °C.

Both grain growth behaviors were identified using the experimental sintering data. The resulting sintering/grain growth model was used to predict the optimized sintering cycle which was too long to be completely explored experimentally (more than 10 hrs). We determined through the two step sintering approach different sintering trajectories, and the optimal sintering cycle has been identified. The experimental verification of the optimal sintering cycle predicted by modeling rendered the average grain sizes close to the ones predicted by modeling and a high degree of densification. The experimentally observed localized porosity probably originated from the specimen cold pressing preparation.

Declaration of Competing Interests

None.

Acknowledgements

The support of the NSF Division of Materials Research (Grant DMR-1900876) is gratefully acknowledged.

References

[1] L. Jiang, Y. Liao, Q. Wan, W. Li, Effects of sintering temperature and particle size on the translucency of zirconium dioxide dental ceramic, J. Mater. Sci. Mater. Med. 22 (2011) 2429–2435, doi: 10.1007/s10856-011-4438-9.
[2] H.B. Zhang, B.-N. Kim, K. Morita, H. Yoshida, J.-H. Lim, K. Hiraga, Optimization of high-pressure sintering of transparent zirconia with nano-sized grains, J. Alloys. Compd. 508 (2010) 196–199, doi: 10.1016/j.jallcom.2010.08.045.
[3] M.-J. Kim, J.-S. Ahn, J.-H. Kim, H.-Y. Kim, W.-C. Kim, Effects of the sintering conditions of dental zirconia ceramics on the grain size and translucency, J. Adv. Prosthodont. 5 (2013) 161, doi: 10.4047/jap.2013.5.2.161.
[4] C. Piconi, G. Maccauro, Zirconia as a ceramic biomaterial, Biomaterials 20 (1999) 1–25, doi: 10.1016/S0142-9612(98)00010-6.
[5] I. Denry, J. Kelly, State of the art of zirconia for dental applications, Dent. Mater. 24 (2008) 299–307, doi: 10.1016/j.dental.2007.05.007.
[6] M.N. Rahaman, Sintering of Ceramics, CRC Press, 2007.
[7] R.M. German, Sintering Theory and Practice, Wiley, Wiley, 1996 http://www.wiley.com/WileyCDA/WileyTitle/productCd-047105786X.html .
[8] C. Manière, L. Durand, A. Weibel, C. Estournès, Spark-plasma-sintering and finite element method: from the identification of the sintering parameters of a submicronic α -alumina powder to the development of complex shapes, Acta Mater 102 (2016) 169–175, doi: 10.1016/j.actamat.2015.09.003.
[9] E.A. Olevsky, Theory of sintering: from discrete to continuum, Mater. Sci. Eng. R Reports. 23 (1998) 41–100, doi: 10.1016/S0927-796X(98)00009-6.
[10] R.K. Bordia, S.-J.L. Kang, E.A. Olevsky, Current understanding and future research directions at the onset of the next century of sintering science and technology, J. Am. Ceram. Soc. 100 (2017) 2314–2352, doi: 10.1111/jace.14919.
[11] E.A. Olevsky, C. Garcia-Cardona, W.L. Bradbury, C.D. Haines, D.G. Martin, D. Kapoor, Fundamental aspects of spark plasma sintering: II. finite element analysis of scalability, J. Am. Ceram. Soc. 95 (2012) 2414–2422, doi: 10.1111/j.1551-2916.2012.05096.x.
[12] E.A. Olevsky, D.V Dudina, Field-Assisted Sintering, Springer International Publishing, Cham, 2018, doi: 10.1007/978-3-319-76032-2.
[13] C. Manière, L. Durand, A. Weibel, C. Estournès, A predictive model to reflect the final stage of spark plasma sintering of submicronic α-alumina, Ceram. Int 42 (2016) 9274–9277, doi: 10.1016/j.ceramint.2016.02.048.
[14] I.-W. Chen, X.-H. Wang, Sintering dense nanocrystalline ceramics without final-stage grain growth, Nature 404 (2000) 168–171, doi: 10.1038/35004548.
[15] V.V. Skorohod, Rheological basis of the theory of sintering, Nauk. Dumka, Kiev (1972).
[16] J. Besson, M. Abouaf, Grain growth enhancement in alumina during hot isostatic pressing, Acta Metall. Mater 39 (1991) 2225–2234, doi: 10.1016/0956-7151(91)90004-K.
[17] Z.-Z. Du, A.C.F. Cocks, Constitutive models for the sintering of ceramic components—I. Material models, Acta Metall. Mater. 40 (1992) 1969–1979, doi: 10.1016/0956-7151(92)90183-F.
[18] L. Dejonghe, M. Rahaman, 4.1 Sintering of ceramics, Handb. Adv. Ceram. (2003) 187–264, doi: 10.1016/B978-012654640-8/50006-7.
[19] F. Raether, P. Schulze Horn, Investigation of sintering mechanisms of alumina using kinetic field and master sintering diagrams, J. Eur. Ceram. Soc. 29 (2009) 2225–2234, doi: 10.1016/j.jeurceramsoc.2009.01.025.
[20] J. Wang, R. Raj, Estimate of the activation energies for boundary diffusion from rate-controlled sintering of pure alumina, and alumina doped with zirconia or titania, J. Am. Ceram. Soc. 73 (1990) 1172–1175, doi: 10.1111/j.1151-2916.1990.tb05175.x.
[21] R.L. Coble, Sintering crystalline solids. I. intermediate and final state diffusion models, J. Appl. Phys 32 (1961) 787–792, doi: 10.1063/1.1736107.
[22] C. Herring, Effect of change of scale on sintering phenomena, J. Appl. Phys. 21 (1950) 301–303, doi: 10.1063/1.1699658.
[23] J.D. Hansen, R.P. Rusin, M.-H. Teng, D.L. Johnson, Combined-Stage sintering model, J. Am. Ceram. Soc. 75 (1992) 1129–1135, doi: 10.1111/j.1151-2916.1992.tb05549.x.
[24] H. Su, D.L. Johnson, Master sintering curve: a practical approach to sintering, J. Am. Ceram. Soc. 79 (1996) 3211–3217, doi: 10.1111/j.1151-2916.1996.tb08097.x.
[25] S.J. Park, P. Suri, E. Olevsky, R.M. German, Master sintering curve formulated from constitutive models, J. Am. Ceram. Soc. 92 (2009) 1410–1413, doi: 10.1111/j.1551-2916.2009.02983.x.
[26] Tosoh, Web page, (2020). https://www.tosoh.com/our-products/advanced-materials/zirconia-powders.
[27] M.I. Mendelson, Average grain size in polycrystalline ceramics, J. Am. Ceram. Soc. 52 (1969) 443–446, doi: 10.1111/j.1151-2916.1969.tb11975.x.
[28] E.A. Olevsky, S. Kandukuri, L. Froyen, Consolidation enhancement in spark-plasma sintering: impact of high heating rates, J. Appl. Phys. 102 (2007) 114913, doi: 10.1063/1.2822189.
[29] R. Chaim, Activation energy and grain growth in nanocrystalline Y-TZP ceramics, Mater. Sci. Eng. A. 486 (2008) 439–446, doi: 10.1016/j.msea.2007.09.022.